AO03: Helmholtz Decomposition of Southern Ocean Winds in an Idealised Global Ocean Model

Ong, Qing Yee Ellie

Supervisor: Prof. David Marshall

Abstract

This report details an exploration into the effect of Southern Ocean winds on the Antarctic Circumpolar Current (ACC). A successive over-relaxation solver programmed by the author is used to compute the streamfunction in an idealised global ocean with wind forcing. The project is split into two parts: 1) applying Helmholtz Decomposition to Southern Ocean winds and 2) shifting Southern Ocean winds both equatorward and poleward to explore potential influences of Southern Ocean winds on large scale ocean circulation. We find using Helmholtz Decomposition that the ACC flow in this idealised global ocean can be largely attributed to the rotational component of wind forcing, with only a small correction from the Coriolis force. This is contrasted by the wind-driven gyres north of the Southern Ocean, which have a circulation determined by the balance between the rotational component of wind forcing and the Coriolis force. In addition, shifting Southern Ocean winds in this idealised case is shown to result in a weakened ACC, as well as weakened gyres in the rest of the ocean for both the poleward and equatorward shift.

1 Introduction

The Antarctic Circumpolar Current (ACC) is an ocean current flowing clockwise around the Antarctic continent. It is the largest ocean current on Earth, with a canonical average flow of 134 Sv (1 Sv = 10^6 m^3 s^{-1}) [1] and measured flows of up to 173 Sv [2]. It is primarily driven by strong westerly winds (blowing from west to east), resulting in an overturning circulation (circulation in the vertical plane) and an eastward flow overall [3]. Changes in the Southern Hemisphere westerly winds can also influence eddy formation in the Southern Ocean [4], which can in turn affect overturning circulations, carbon cycles and ocean acidification rates [5].

Idealised models of wind-driven streamfunctions of the ACC were developed in the late 1960s and early 1970s [6] [7] for cases with realistic coastlines and in a rectangular basin. The model used in this project is based on these studies and is outlined in section 2.2. It includes contributions from the Coriolis force and wind stress but excludes the effect of bathymetry, stratification and eddies.

In this project, Helmholtz Decomposition will be used to separate rotational and divergent components of wind forcing in this two-dimensional model of ocean circulation, allowing for an alternative visualisation of the wind forcing. The application of this method to a wind-driven circulation in a square basin is outlined in [8], which illustrated the relationship between the Coriolis force and rotational component of wind forcing in the vorticity balance and their contribution to western boundary currents. Specifically, [8] showed that the Coriolis forcefunction causes a northward acceleration on the western boundary, directly causing western-intensification of boundary currents. We will attempt to replicate this finding in the context of a global ocean with a simplified coastline.

The second part of this project aims to explore the effect of shifting Southern Ocean winds on the global ocean circulation in an idealised ocean model. Southern Ocean winds have moved polewards and increased in intensity under climate change, and are projected to continue in this pattern [9]. It has also been shown that position of Southern Ocean winds were further north in past glacial climate [10]. This project will explore the impact of poleward and equatorward shifts of Southern Ocean winds on large-scale circulations in an idealised global ocean basin.

Section 2 outlines the theory behind the idealised model used, Helmholtz Decomposition and the rotational forcefunction. Section 3 discusses the numerical method and theoretical reasoning behind the computation of the streamfunction. Section 4.1 discusses results of the Helmholtz Decomposition of Southern Ocean winds, and section 4.2 discusses the impact of an equatorward and poleward shift in Southern Ocean winds on the streamfunction. Section 5 summarises the main conclusions and possible further work.

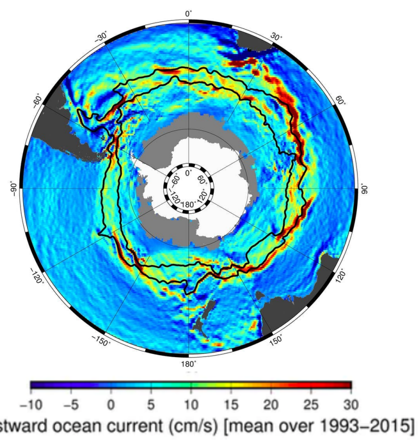

Figure 1: *Eastward current around Antarctica in the Antarctic Circumpolar Current. Reproduced from [11].*

2 Theory

2.1 The Stommel Model

This idealised ocean experiment makes use of the Stommel model [12] as described by equation (1); a vorticity equation taking into account the balance of vorticity between wind stress, the Coriolis force and frictional dissipation:

$$\beta \frac{\partial \psi}{\partial x} = \frac{\boldsymbol{k} \cdot (\nabla \times \boldsymbol{\tau})}{\rho H} - r\nabla^2 \psi. \tag{1}$$

(1) can be solved to obtain the streamfunction ψ in an ocean basin forced by wind stress τ and the Coriolis force, quantified by the Coriolis parameter β. Here, ρ is the mean density of water in the ocean, H is the depth of the ocean, assumed to be constant, $\boldsymbol{k}$ is the unit vector in the upwards direction on the earth's surface, x is the coordinate in the eastward direction and r is a coefficient of friction, where we assume friction is parameterised by a linear drag. This is shown explicitly in the horizontal momentum equation (18), where there is a frictional term included that is linear to velocity $\boldsymbol{u}$.

The first term on the right-hand side of (1) represents surface winds acting as a source of vorticity, and the second term is the vorticity sink due to energy dissipation from friction. The term on the left is the vorticity advection term, representing the transport of planetary vorticity by the flow, and we also assume that the Rossby number of this system is small so that relative vorticity can be neglected.

2.2 Helmholtz Decomposition and the Rotational Forcefunction

Helmholtz Decomposition uses Helmholtz's theorem, which states that any force can be separated into two components; rotational and divergent:

$$\boldsymbol{F} = \boldsymbol{F_{rot}} + \boldsymbol{F_{div}}, \tag{2}$$

where

$$\nabla \cdot \boldsymbol{F_{rot}} = 0, \quad \nabla \times \boldsymbol{F_{div}} = 0.$$

This decomposition, although not realistic, is linear and hence can provide a conceptual understanding of the system more readily. This is particularly helpful when considering the flows in ocean, where the divergent component of wind forcing is countered by the pressure gradient forces established in response to the winds. Hence, rather than considering the effect of wind forcing on pressure gradients formed and any resulting fluid flow, we only need to consider the effect of the rotational component of wind forcing on fluid flow. Thus for this experiment, we do not have to take pressure gradients into account if applying the rotational component of wind forcing on our system. This is illustrated in figure 2.

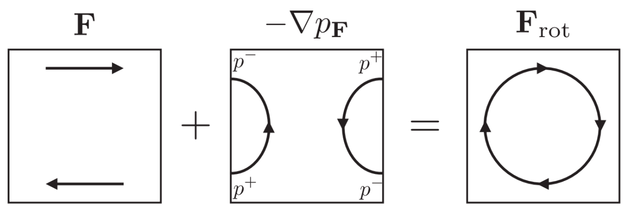

Figure 2: *Schematic showing the sum of the applied zonal force and pressure gradients formed resulting in a rotational force. Reproduced from [8].*

Specifically, the rotational component of force is projected onto local acceleration, where $\boldsymbol{u}$ is the velocity,

$$\boldsymbol{F_{rot}} = \rho \frac{\partial \boldsymbol{u}}{\partial t}, \tag{3}$$

whereas, the divergent component of force is projected onto the pressure gradient.

$$\boldsymbol{F_{div}} = \nabla p. \tag{4}$$

Hence when solving for ψ, only the rotational component needs to be taken into account as the divergent component of the wind forcing will vanish in (1).

We can also define a rotational forcefunction ϕ_F by (5), such that the rotational forcefunction is analogous to a streamfunction with a 'velocity field' of $\boldsymbol{F_{rot}}$:

$$\frac{\boldsymbol{F_{rot}}}{\rho} = \boldsymbol{k} \times \nabla \phi_F. \tag{5}$$

This allows us to solve for the second order differential equation (6) to obtain the forcefunction in this domain:

$$\nabla^2 \phi_F = \frac{\boldsymbol{k}}{\rho} \cdot (\nabla \times \boldsymbol{\tau}). \tag{6}$$

3 Method of Solution

3.1 Successive Over-Relaxation

The numerical method used to solve for the streamfunction is successive over-relaxation (SOR) and a bespoke solver was developed and coded specifically for this project, the development of which was a substantial task. SOR is one of many relaxation methods for boundary-value problems and was chosen for ease of coding and to avoid diverging solutions [13]. A physical explanation of relaxation methods is as follows:

Consider an elliptic equation where we wish to solve for a quantity u, with L representing an elliptic operator and ρ representing a source term:

$$Lu = \rho. \tag{7}$$

We can interpret (7) as the steady state case of a diffusion equation as such:

$$\frac{\partial u}{\partial t} = Lu - \rho. \tag{8}$$

Applying this to Stommel equation (1) at each spatial point (i, j) where we want to solve for ψ, we obtain:

$$\frac{\psi_{i,j}^{n+1} - \psi_{i,j}^{n}}{\Delta t} = (\nabla^2 \psi)_{i,j}^{n} + \frac{\beta}{r} (\frac{\partial \psi}{\partial x})_{i,j}^{n} - \frac{(\boldsymbol{k} \cdot (\nabla \times \boldsymbol{\tau}))_{i,j}^{n}}{\rho H r}. \tag{9}$$

By iterating over 'time-steps' n of width Δt, the initial distribution of ψ *relaxes* to an equilibrium solution as $t \to \infty$, taking into account the Coriolis and wind stress terms.

Now, we can use finite differencing to calculate the $(\nabla^2 \psi)_{i,j}^{n}$ and other terms on the right side of the equation. Finite differencing approximates derivatives as $f'(x) \approx \frac{f(x+\Delta x) - f(x)}{\Delta x}$ for small Δx, such that derivatives are dependent on the values of the function on adjacent grid cells. This allows us to write a general elliptic equation in terms of the quantity being calculated on the current grid cell and its adjacent grid cells. To apply SOR to a general second-order elliptic equation in x and y

coordinates, finite differenced on a square, we write the elliptic equation as follows:

$$\begin{aligned} &a_{i,j}u_{i+1,j} + b_{i,j}u_{i-1,j} + \\ &\quad c_{i,j}u_{i,j+1} + d_{i,j}u_{i,j-1} + e_{i,j}u_{i,j} = f_{i,j}, \end{aligned} \tag{10}$$

with coefficients a, b ... f being set based on the original elliptic equation. For example, for our equation (9), $f_{i,j}$ is proportional to the vorticity source term.

The next iteration is computed by solving for $u_{i,j}$ and taking a weighted average of the old $u_{i,j}$ and iterated $u_{i,j}$:

$$\begin{aligned} u^*_{i,j} =& \frac{1}{e_{i,j}}(f_{i,j} - a_{i,j}u_{i+1,j} - b_{i,j}u_{i-1,j} \\ &- c_{i,j}u_{i,j+1} - d_{i,j}u_{i,j-1}), \end{aligned} \tag{11}$$

and

$$u^{new}_{i,j} = \omega u^*_{i,j} + (1-\omega)u^{old}_{i,j}. \tag{12}$$

Each iteration of $u_{i,j}$ is calculated as:

$$u^{new}_{i,j} = u^{old}_{i,j} + \omega\frac{\xi_{i,j}}{e_{i,j}}, \tag{13}$$

where the residual $\xi_{i,j}$ is determined by:

$$\begin{aligned} \xi_{i,j} =& a_{i,j}u_{i+1,j} + b_{i,j}u_{i-1,j} + c_{i,j}u_{i,j+1} \\ &+ d_{i,j}u_{i,j-1} + e_{i,j}u_{i,j} - f_{i,j}, \end{aligned} \tag{14}$$

Here, ω is the over-relaxation parameter and this method is only convergent for $0 < \omega < 2$. We chose a value of ω through trial and error, such that ω is small enough that the solution will converge but large enough to optimise for the speed of the program. SOR also makes use of the Gauss-Seidel method of updating the calculated values at each grid cell as they are calculated, rather than replacing all the values after each iteration [13].

For our idealised ocean model, coastlines have been defined to have $\psi = 0$ at the boundary, with a non-zero streamfunction on the Southern boundary to account for a non-zero flow at Antarctica. A spherical surface with realistic coastlines, based on observational data, has been defined and the boundaries have been simplified for easier calculation as detailed in section 3.2. This simplification of coastlines required modest manual intervention to ensure that there was only one island left in the domain: Antarctica. This ensured that the balance of circulation forced by wind stress and rate of flow in (19) only had to be implemented at the southern boundary around Antarctica. Full spherical geometry was used when solving for the streamfunction and the coefficient of friction has been chosen such that the control state has a rate of transport comparable to the ACC in the ocean, setting r = 1.5 x $10^{-6}s^{-1}$.

3.2 Solving for the Streamfunction

To solve for streamfunction ψ in a multiply connected domain, such as a global ocean with land boundaries, the method outlined in [14] is utilised. This method is easier to implement with fewer 'islands', hence the coastlines are simplified resulting in one island, the Antarctic continent, and the outer boundary is defined by the joined-up coastline of all other landmasses. A summary of the method used is given below.

The solution of (1) is separated into the particular integral ψ_{PI} and complementary function ψ_{CF}, with a constant b:

$$\psi = \psi_{PI} + b\psi_{CF}. \tag{15}$$

The particular integral and complementary function are defined as follows:

$$r\nabla^2\psi_{PI} + \beta\frac{\partial\psi_{PI}}{\partial x} = \frac{\boldsymbol{k}\cdot(\nabla\times\boldsymbol{\tau})}{\rho H}, \tag{16}$$

with $\psi_{PI} = 0$ on all boundaries; and

$$r\nabla^2\psi_{CF} + \beta\frac{\partial\psi_{CF}}{\partial x} = 0, \tag{17}$$

with $\psi_{CF} = 1$ at the southern boundary and $\psi_{CF} = 0$ on the remaining boundaries, such that the complementary function ψ_{CF} is solved for with a non-zero streamfunction at the Antarctic continental shelf and zero flow in and out of other land masses.

We then need to chose b such that the system is in balance in the momentum and vorticity equations. Now we start with the horizontal momentum equation in steady state (18):

$$(\boldsymbol{u}\cdot\nabla)\boldsymbol{u}+f\boldsymbol{k}\times\boldsymbol{u}+\frac{1}{\rho}\nabla p=\frac{\boldsymbol{\tau}}{\rho H}-r\boldsymbol{u}. \tag{18}$$

Rewriting (18) in vector-invariant form and evaluating the circulation around the southern boundary, the pressure gradient and Coriolis terms will vanish, leaving only the balance between the circulation forced by wind stress and rate of flow in (19). Hence, the scaling constant b is chosen such that the circulation forced by wind stress is balanced by the rate of flow around the southern boundary:

$$\frac{1}{\rho H}\oint\boldsymbol{\tau}\cdot d\boldsymbol{l}=r\oint\boldsymbol{u_{PI}}\cdot d\boldsymbol{l}+b\left(r\oint\boldsymbol{u_{CF}}\cdot d\boldsymbol{l}\right). \tag{19}$$

To compute the streamfunction and circulations, we use masks to define areas of land, ocean and coastlines. This enables us to integrate over the whole basin and also neglect values that were not relevant to the calculation. For example, we can neglect areas of land when calculating the streamfunction in the ocean using SOR, as well as only including grid cells along the southern boundary when calculating the circulation in (19).

4 Results

4.1 Rotational Forcefunction on the Global Ocean

The streamfunction ψ was computed using realistic wind stress data using the method in section 3 and the results are shown in figure 3. In the top panel, gyres in the northern and southern Hemispheres are formed in each of the oceans, and the ACC is also shown with a rate of transport ranging from 60-160 Sv. This is consistent with other experiments of a global ocean circulation for an ocean with homogeneous density and uniform depth, such as in [6].

The rotational and Coriolis forcefunctions of a wind-driven no-slip gyre were computed and plotted in figure 7 of [8]. This showed that the Coriolis force causes a northward acceleration at the western boundary, directly causing western intensification. For our experiment, we can also attempt to replicate this result by defining a Coriolis forcefunction similar to the rotational forcefunction, which is analogous to a streamfunction with a 'velocity field' of the Coriolis force:

$$\nabla^2\phi_\beta=\beta\frac{\partial(H\psi)}{\partial x}. \tag{20}$$

Hence, the Stommel equation (1) can be rewritten as:

$$\frac{1}{Hr}\nabla^2\phi_\beta=\frac{1}{Hr}\nabla^2\phi_F-\nabla^2\psi. \tag{21}$$

Therefore, we can obtain a relationship between the forcefunctions and streamfunction, being careful to take the boundary conditions into account. Writing this relationship in terms of the rate of transport $H\psi$,

$$H\psi=\frac{1}{r}(\phi_\beta+\phi_F). \tag{22}$$

From here, we can calculate the rotational forcefunction ϕ_F using (6), followed by computing the Coriolis forcefunction ϕ_β using (22). We see in (22) that the rotational forcefunction and Coriolis forcefunction each contribute to the total rate of transport when scaled by a factor of $1/r$. Thus we can plot ϕ_F/r, the scaled rotational forcefunction corresponding to the rate of transport due to the rotational component of wind stress; and ϕ_β/r, the scaled Coriolis forcefunction corresponding to the rate of transport due to the Coriolis force, as shown in figure 3. Here, the forces are directed along contours of the forcefunction plots, at a strength inversely proportional to the spacing between contours lines.

The scaled rotational forcefunction plot is similar to the streamfunction plot but without western intensification. However in the scaled Coriolis forcefunction plot, there are large accelerations next to the western boundary in the ocean basins north of the Southern Ocean, which are unfortunately masked in the plot as the acceleration occurs over the final grid point (see an example in grey box in the bottom panel of figure 3). This indicates that in the horizontally bounded ocean basins, the Coriolis forcefunction is causing a northward acceleration along the western boundary to produce a boundary current, which is consistent with the results in [8].

In contrast, in the Southern Ocean, the ACC is almost entirely forced by the rotational forcefunction, whereas the contribution to the total rate of transport by the Coriolis forcefunction is small. This indicates that in this idealised model, the ACC is almost entirely dependent on the rotational component of the wind stress and the Coriolis force has very little effect.

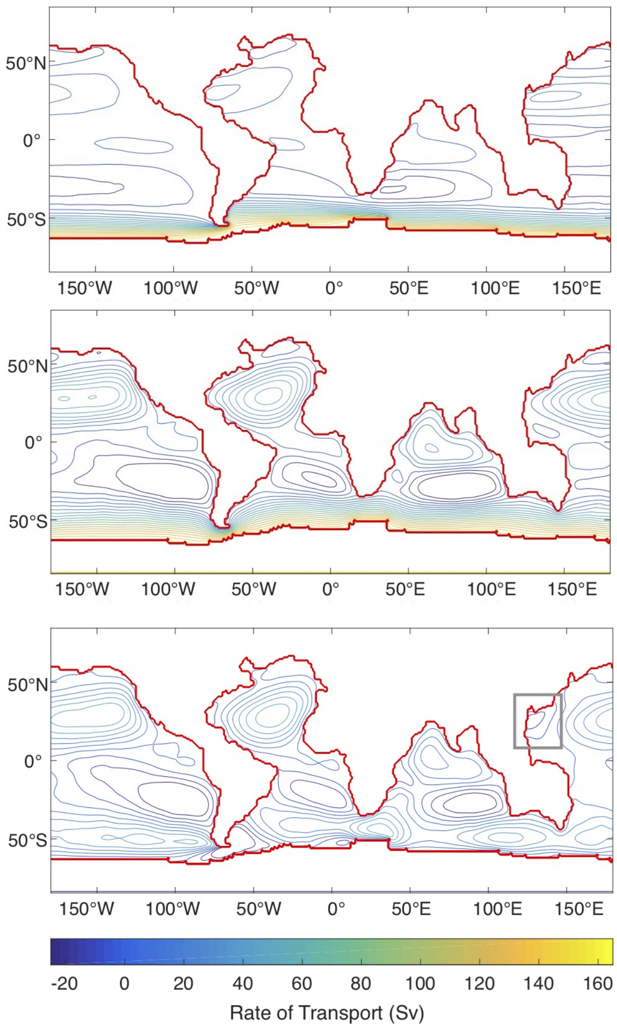

Figure 3: *Rate of transport $H\psi$ (top), scaled rotational forcefunction ϕ_F/r (middle) and scaled Coriolis forcefunction ϕ_β/r (bottom) for an idealised global ocean in Sverdrups (1 Sv = 10^6 m^3 s^{-1}), with contour intervals of 10 Sv. The grey box in the scaled Coriolis forcefunction plot highlights the region of large northward acceleration at the western boundary, which is masked in the plot as the acceleration occurs over the final grid point.*

4.2 Shifting Southern Ocean Winds

To explore the effect of shifting Southern Ocean winds, we now shift the peak of zonal mean observed winds by 10°, as shown in figure 4, and extrapolate this shift to the full spatial wind stress vector field. Using these shifted wind stress fields, we can calculate the streamfunction and forcefunctions resulting from these modified wind forcings and scaling them to represent the rates of transport, with the results for an equatorward shift in figure 5 and the results for a poleward shift in figure 6.

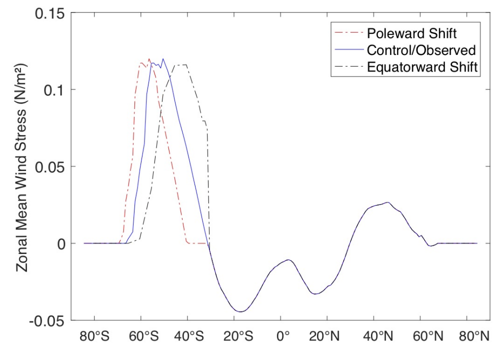

Figure 4: *Zonally-averaged wind stress with latitude for wind stress data used in experiments.*

Looking at the case of Southern Ocean winds being shifted equatorward in figure 5, the ACC has weakened significantly (from a maximum rate of transport of approximately 160 Sv originally to a maximum 80 Sv). Additionally, the gyres in all of the basins have weakened as well when compared to the control case with observed winds, and the feature of western boundary currents is also seen in the scaled Coriolis forcefunction plot.

For the case of Southern Ocean winds being shifted polewards in figure 6, the gyres in the Northern Hemisphere and the ACC flow have weakened when compared to the control case with observed winds. However, the ACC is not as weak as in the case of equatorward shifted winds. The position of the gyres in the streamfunction and forcefunctions plots are unchanged after the shifting of winds, and the feature of western boundary currents in the scaled Coriolis forcefunction plot is still visible.

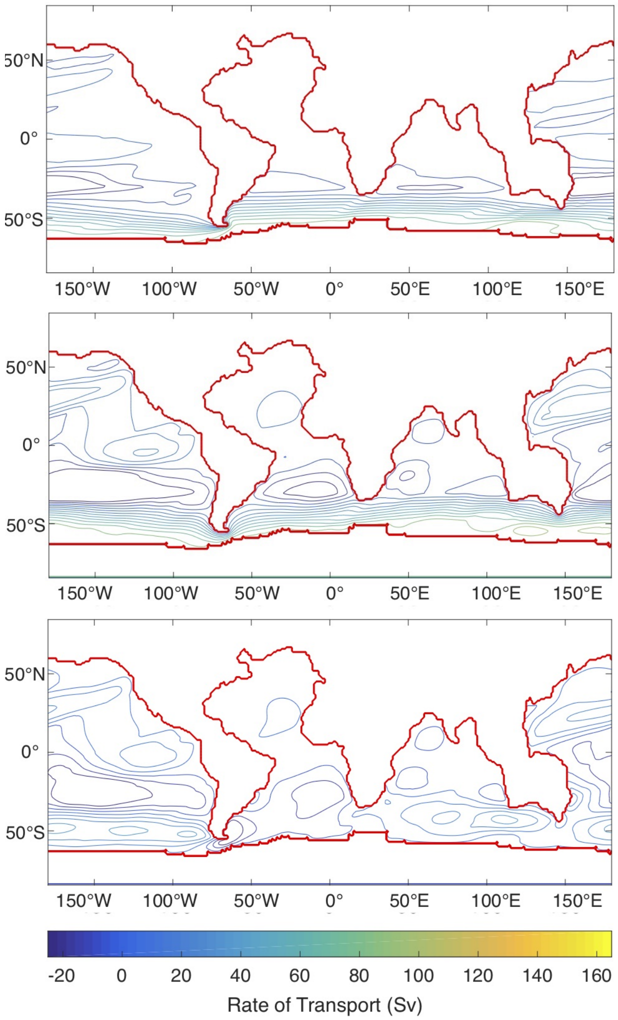

Figure 5: *Rate of transport $H\psi$ (top), scaled rotational forcefunction ϕ_F/r (middle) and scaled Coriolis forcefunction ϕ_β/r (bottom) for an idealised global ocean in Sverdrups, with contour intervals of 10 Sv.*

Investigating the weakened gyres in the Northern Hemisphere with the shifting of winds further, we can consider the particular integral and complimentary function of the streamfunction as in (16). The particular integral of the streamfunction ψ_{PI} is analogous to the streamfunction in the ocean if the boundary condition on the bottom boundary (at the Antarctic continent) is $\psi = 0$ such that the ocean is a closed basin. The particular integral of the streamfunction in each of the three scenarios of wind stress are shown in figure 7.

The gyres in the Atlantic and Indian Oceans are already weakened in ψ_{PI} when the winds are shifted. This might be explained by the changes in the large gyre crossing the Atlantic and Indian Ocean. Considering the plot for the case of observed winds, we can see that a large gyre circulating anticlockwise in the Southern Ocean is formed, crossing the southern Atlantic and Indian Oceans. However, looking at the streamfunction plot for equatorward shifted winds, this gyre is now circulating clockwise, forming an additional vorticity sink such that other gyres must weaken to conserve vorticity. Similarly, as the Southern Ocean winds are shifted polewards, weaker winds end up at the boundary of the Antarctic continent and the ocean, such that a weaker gyre circulating anticlockwise is formed. Hence, this must result in weaker gyres circulating clockwise in the rest of the ocean in order for vorticity to be conserved overall. However, there was insufficient time to determining the exact mechanical process that results in the weaker gyres. Hence, this would be an obvious focus for further work if there were any more time.

5 Conclusions and Further Work

This project set out with two aims: 1) to use the Helmholtz Decomposition method to investigate the rotational component of winds and 2) to explore the effect of shifting Southern Ocean winds on rate of transport in an idealised global ocean. We used the simplest possible model to carry out the experiments in order to capture the basic physics and aid our conceptual understanding, while still producing results that were relevant to the ocean.

For the Helmholtz Decomposition of Southern Ocean winds, we show that the circulation in wind-driven gyres is determined by the balance between the rotational component of wind stress and the Coriolis force, which is consistent with results from the wind-driven no-slip gyres in [8]. However, this is completely different from the Southern Ocean, where we find that the ACC flow is almost entirely driven by the rotational component of wind stress, with only a small contribution from the Coriolis force.

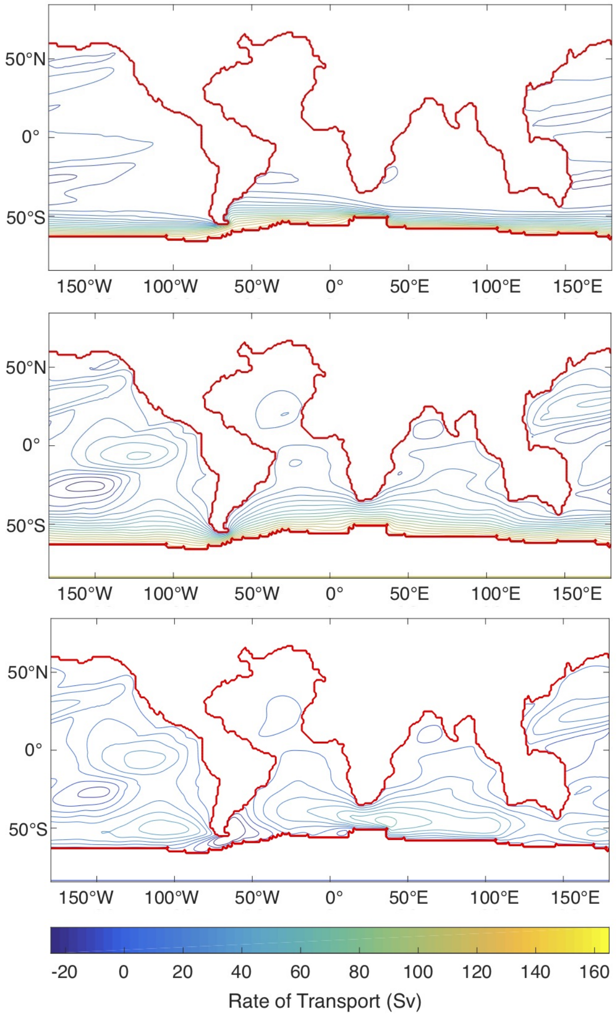

Figure 6: *Rate of transport $H\psi$ (top), scaled rotational forcefunction ϕ_F/r (middle) and scaled Coriolis forcefunction ϕ_β/r (bottom) for an idealised global ocean in Sverdrups, with contour intervals of 10 Sv.*

Looking at shifting Southern Ocean winds, we find that the ACC weakened in both cases. For the equatorward shift in wind, the rotational forcefunction gives a smaller ACC flow that is further north compared to the case with observed winds. This can be attributed to the lack of winds acting at the southern boundary and hence the reduced wind forcing available to drive the ACC. For the poleward shift in winds, the rotational forcefunction gives a slightly weaker ACC compared to the case with observed winds. This contradicts the literature as the ACC was predicted either to strengthen with a poleward shift of Southern Ocean winds [15] [16] or that ACC transport is insensitive to decadal changes in wind stress [17]. This is likely due to the Southern Ocean winds acting on the masked area of land as well as the idealised ocean, resulting in a weaker ocean circulation. This issue could be eliminated in future work with a more accurate coastline of Antarctica or greater coverage of wind stress data in the Southern Ocean region to allow for a more useful poleward Southern Ocean windshift experiment.

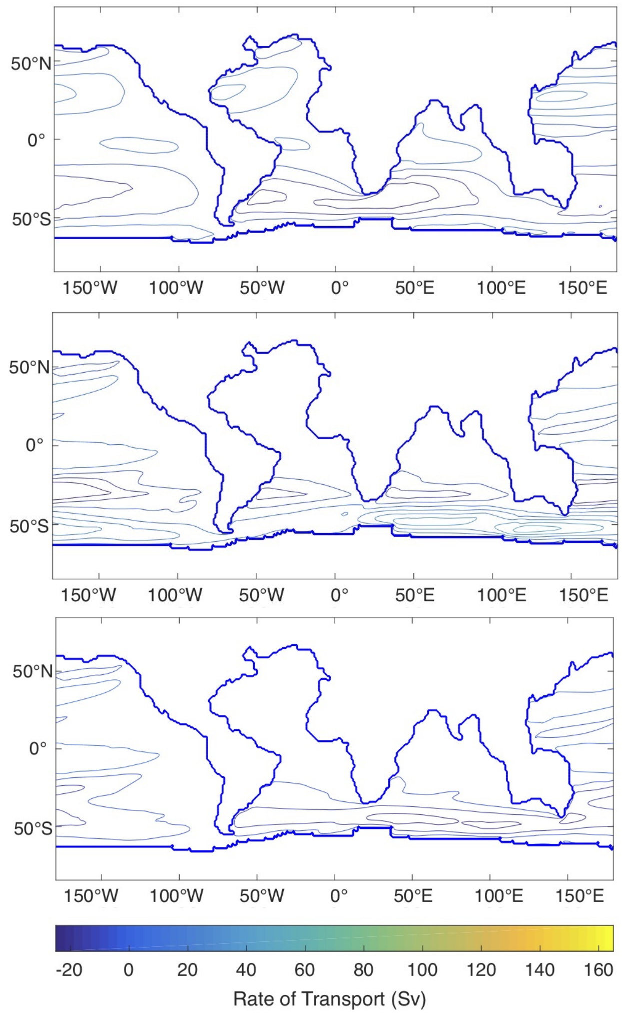

Figure 7: *ψ_{PI} for observed winds (top), winds shifted equatorward (middle) and wind shifted polewards (bottom) in Sverdrups with contour intervals of 10 Sv.*

As seen in figure 7, the strength and structure of the gyres in the Northern Hemisphere is directly related by changes in wind forcing in the Southern Ocean. This also agrees with [18], which found that wind stresses above the Drake Passage latitude were important in setting the strength of the ACC. These changes are necessary in order to conserve vorticity, however the particular mechanism by which the gyres in the Northern Hemisphere are modified by winds in the Southern Ocean is not dealt with in this project. Investigating if this weakening effect can be seen outside the context of idealised ocean models and understanding the specific mechanisms involved would be an interesting focus of future work.

The model used in this project did not take density variations into account. The forcefunction approach is currently only defined for the case of a Boussinesq fluid and so to take density variations into account, further work is required to define an additional "overturning" forcefunction. We have also assumed a flat bottom basin, whereas in the Southern Ocean, bottom topography contributes significantly to eddy formation and the flow of the ACC [4]. There are also influences in ice-ocean interactions that are not accounted for [19] [20]. Including each of the above variables would tremendously increase the scope and complexity of the project, however, exploring how forcefunctions can be used in more complex models would be an intriguing area for future work.

For the SOR solver, we chose a value of ω small enough such that the solution would converge and large enough that the speed of the code would be optimised. There are potentially alternatives for being more precise with the choice of ω , however due to the simplicity of the model, finding the exact optimum ω value would probably have been overkill. This would have to be taken into consideration if the model were made more complex, for example, using a higher resolution or including additional islands, as speed of the solver would then be a bigger issue. Alternatively, further work might incorporate a multi-grid or conjugate gradient solver to improve computing speeds [13].

References

[1] T. Whitworth and R. G. Peterson, "Volume Transport of the Antarctic Circumpolar Current from Bottom Pressure Measurements," *Journal of Physical Oceanography*, vol. 15, 1984.

[2] K. A. Donohue, K. L. Tracey, D. R. Watts, M. P. Chidichimo, and T. K. Chereskin, "Mean Antarctic Circumpolar Current transport measured in Drake Passage," *Geophysical Research Letters*, vol. 43, pp. 760–11, 11 2016.

[3] Geoffrey K. Vallis, *Essentials of Atmospheric and Oceanic Dynamics.* Cambridge: Cambridge University Press, 2019.

[4] A. M. C. Hogg, M. P. Meredith, D. P. Chambers, E. P. Abrahamsen, C. W. Hughes, and A. K. Morrison, "Recent trends in the Southern Ocean eddy field," *Journal of Geophysical Research: Oceans*, vol. 120, no. 1, pp. 257–267, 2015.

[5] L. Xue, W. J. Cai, T. Takahashi, L. Gao, R. Wanninkhof, M. Wei, K. Li, L. Feng, and W. Yu, "Climatic modulation of surface acidification rates through summertime wind forcing in the Southern Ocean," *Nature Communications*, vol. 9, 12 2018.

[6] K. Bryan and M. Cox, "The Circulation of the World Ocean: A Numerical Study. Part I, A Homogenous Model," *Journal of Physical Oceanography*, pp. 319–355, 1972.

[7] A. E. Gill, "A Linear Model of Antarctic Circumpolar Current," *Journal of Fluid Mechanics*, vol. 32, part 3, pp. 465–488, 1968.

[8] D. P. Marshall and H. R. Pillar, "Momentum Balance of the Wind-Driven and Meridional Overturning Circulation," *Journal of Physical Oceanography*, vol. 41, pp. 960–978, 2011.

[9] D. W. J. Thompson and S. Solomon, "Interpretation of Recent Southern Hemisphere Climate Change," *Science*, vol. 296, pp. 895 – 899, 2002.

[10] J. R. Toggweiler, J. L. Russell, and S. R. Carson, "Midlatitude westerlies, atmospheric CO2, and climate change during the ice ages," *Paleoceanography*, vol. 21, 6 2006.

[11] H. Phillips, B. Legresy, and N. Bindoff, "Explainer: how the Antarctic Circumpolar Current helps keep Antarctica frozen," *The Conversation*, 2018.

[12] H. Stommel, "The Westward Intensification of Wind-Driven Ocean Currents," *Transactions, American Geophysical Union*, 1948.

[13] W. Press, S. Teukolsky, P. Vetterling, and B. Flannery, *Numerical Recipes in Fortran 77: The Art of Scientific Computing Second Edition.* Cambridge University Press, 1992.

[14] J. C. McWilliams, "A Note on a Consistent Quasigeostrophic Model in a Multiply Connected Domain," *Dynamics of Atmospheres and Oceans*, vol. 1, pp. 427–441, 1977.

[15] J. C. Fyfe and O. A. Saenko, "Simulated changes in the extratropical Southern Hemisphere winds and currents," *Geophysical Research Letters*, vol. 33, 3 2006.

[16] D. Bi, S. J. Marsland, P. Uotila, S. O'Farrell, R. Fiedler, A. Sullivan, S. M. Griffies, X. Zhou, and A. C. Hirst, "ACCESS-OM: The ocean and sea-ice core of the ACCESS coupled model," *Australian Meteorological and Oceanographic Journal*, vol. 63, no. 1, pp. 213–232, 2013.

[17] C. W. Böning, A. Dispert, M. Visbeck, S. R. Rintoul, and F. U. Schwarzkopf, "The response of the Antarctic Circumpolar Current to recent climate change," *Nature Geoscience*, vol. 1, pp. 864–869, 12 2008.

[18] L. C. Allison, H. L. Johnson, D. P. Marshall, and D. R. Munday, "Where do winds drive the Antarctic Circumpolar Current?," *Geophysical Research Letters*, vol. 37, 6 2010.

[19] M. A. Depoorter, J. L. Bamber, J. A. Griggs, J. T. Lenaerts, S. R. Ligtenberg, M. R. Van Den Broeke, and G. Moholdt, "Calving fluxes and basal melt rates of Antarctic ice shelves," *Nature*, vol. 502, no. 7469, pp. 89–92, 2013.

[20] F. Alexander Haumann, N. Gruber, M. Münnich, I. Frenger, and S. Kern, "Sea-ice transport driving Southern Ocean salinity and its recent trends," *Nature*, vol. 537, pp. 89–92, 8 2016.